

# FRACTURE BEHAVIOR OF ADDITIVELY MANUFACTURED CEMENTITIOUS MATERIALS

MO LI<sup>\*</sup>, YUN-CHEN WU<sup>\*</sup> AND XINBO WANG<sup>\*</sup>

<sup>\*</sup> University of California, Irvine, Department of Civil and Environmental Engineering  
4145 Engineering Gateway, Irvine, California, USA  
e-mail: moli@uci.edu

**Key words:** Additive manufacturing, cementitious material, fracture toughness, process zone, thixotropy

**Abstract:** Additive manufacturing (AM) of cementitious materials, also known as 3D printing, offers transformative potential for the construction sector. Given the inherently quasi-brittle behavior of cementitious materials and their vulnerability to fracture, it is essential to understand how the layer-by-layer extrusion process affects their fracture resistance. This study explored the interplay between early-age rheology, pore structure, and fracture toughness of additively manufactured cementitious materials. Using three-dimensional micro-computed tomography, the impact of early-age thixotropic behavior and varying printing time intervals on the pore structure of the interlayers was examined. Fracture tests were conducted on printed specimens, incorporating a digital image correlation system for precise monitoring and visualization of crack evolution. The findings demonstrated that fracture toughness of additively manufactured cementitious materials is strongly influenced by their early-age rheological behavior and printing conditions.

## 1 INTRODUCTION

Concrete additive manufacturing (AM), also known as 3D printing, is a layer-by-layer extrusion-deposition process using robotic arms or gantry printers to construct structural components with cementitious materials. During the AM process, fresh-state cementitious materials undergo high shear during extrusion, causing a reduction in viscosity due to the breakdown of the flocculated structure. Once deposited, the shear decreases, leading to the rebuilding of the colloidal network and formation of calcium-silicate-hydrate (C-S-H) bonds, a process described as thixotropy [1,2]. The thixotropic behavior influences the interlayer imperfections and porosity, which in turn affect the mechanical properties including the

fracture behavior of the printed components [3].

Interlayer regions in additively manufactured cementitious materials have been shown to significantly impact mechanical performance, with studies reporting reductions of 20% to 47% in compressive strength and 36% to 90% in flexural strength [4-10]. Factors contributing to these variations include differences in material mix design, printing parameters, and testing methods [3]. The interlayer bonding strength, influenced by printing time intervals, has been found to decrease significantly over time, resulting in weaker mechanical performance [11].

The sensitivity of interlayer properties to printing time intervals highlights the importance of understanding the early-age thixotropic behavior of cementitious materials. This paper presents our study on the effect of

material early-age rheology on the pore structure and fracture behavior of additively manufactured cementitious materials. Three-interval thixotropy tests were performed to measure viscosity changes during different stages of the AM process. Specimens with varying printing time intervals were additively manufactured, and their pore structures and fracture properties were analyzed using 3D micro-CT and fracture toughness tests. By analyzing the changes in rheological properties due to different printing time intervals, this study aims to elucidate the underlying mechanisms affecting the fracture process zone and fracture toughness additively manufactured cementitious materials.

## 2 MATERIALS AND METHODS

Table 1 outlines the compositions of the additively manufactured cementitious material investigated in this study. The mixture contained Type I/II/V ordinary Portland cement, densified silica fume, fine silica sand, ground quartz, water, and a polycarboxylate-based superplasticizer (SP).

The cementitious mixtures were prepared using a 28.4-liter capacity Hobart mixer. Dry components were first mixed for 5 minutes. Subsequently, water, SP, and VMA were combined and added, followed by another 5 minutes of mixing to achieve a homogeneous mortar. The fresh material was printed into specimens using an automated six-degree-of-freedom robotic arm; these specimens were further sectioned into beam specimens with individual beam dimensions of 279.4 mm  $\times$  50.8 mm  $\times$  25.4 mm (Fig. 1). The printing filaments were perpendicular to the length of the beam specimens. Four distinct printing time intervals ( $t_p = 0, 5, 10,$  and 15 minutes) between interlayers were selected to represent typical time delays in large-scale additive manufacturing. After printing, specimens were covered with plastic sheets and moisture-cured for 28 days at a constant temperature of  $23 \pm 1$  °C. A single-edge notch, 16.9 mm deep with a 2-mm opening and 0.08-mm root radius, was introduced at the mid-span of each beam specimen, either at the interlayer or in the

filament, maintaining a notch-to-depth ratio of 1:3 [12]. These notched beams underwent three-point bending tests to evaluate fracture behavior.

**Table 1.** Mix design

Material (kg/m <sup>3</sup> )	
Cement	1017
Silica fume	254
Fine silica sand	580
Ground quartz	30.5
Water	305
SP	13.2

Additionally, smaller samples (10 mm  $\times$  9 mm  $\times$  8 mm), each containing one interlayer, were extracted from the printed specimens for microstructural analysis using X-ray computed microtomography (micro-CT) to investigate the three-dimensional air phase structure.

A thixotropy test was designed to replicate the viscosity changes experienced by cementitious materials during additive manufacturing. The process involved three stages: low initial shear to represent the pre-extrusion phase, high shear during extrusion, and gradual recovery post-deposition. The material was subjected to an initial low shear rate of 0.1 s<sup>-1</sup> for 30 seconds, followed by a rapid increase to 15 s<sup>-1</sup> for 30 seconds to simulate the extrusion process. Subsequently, the shear rate was decreased back to 0.1 s<sup>-1</sup> and maintained for 15 minutes, allowing observation of viscosity recovery over time.

X-ray computed microtomography (micro-CT) was employed to assess and compare the air-phase microstructure in interlayer and filament regions of 10 mm  $\times$  9 mm  $\times$  8 mm samples with a spatial resolution of 10  $\mu$ m. Noise reduction involved wavelet-based denoising and median filtering, after which the air and solid phases were segmented via a machine learning model [3]. The reconstructed 3D images provided a detailed view of void characteristics in interlayers.

Fracture behavior of additively manufactured cementitious materials was

examined through three-point bending tests (Fig. 1) on single-notched beams ( $304.8 \text{ mm} \times 50.8 \text{ mm} \times 25.4 \text{ mm}$ ) after 28 days of curing, following ASTM E399 and RILEM standards [12, 13]. An MTS hydraulic testing frame applied loads with closed-loop displacement control, while digital image correlation (DIC) was used for non-contact, high-resolution 3D displacement measurements [3,14]. Specimens were prepared with a speckle pattern on a white background for DIC tracking. During testing, a controlled loading rate ensured a constant crack mouth opening displacement (CMOD) of  $0.005 \text{ mm/min}$ . The DIC system captured crack initiation and propagation, while the MTS system recorded load data. The test ended upon full fracture, indicated by complete crack propagation across the beam depth.

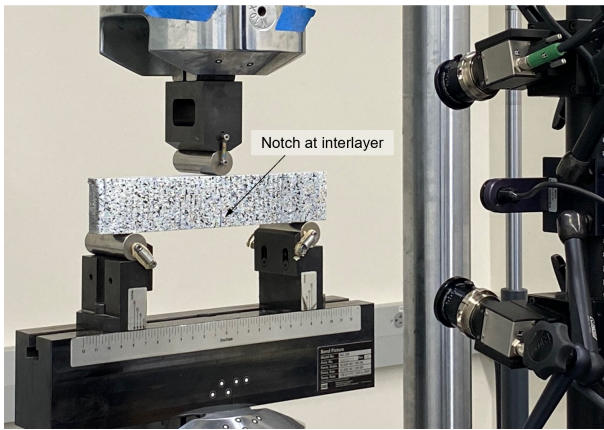


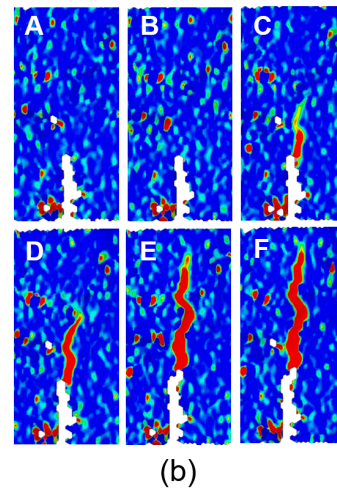
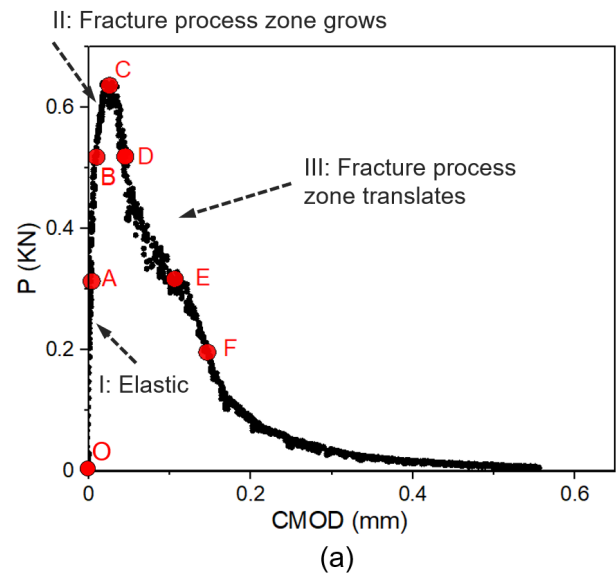
**Figure 1:** Fracture experiment on additively manufactured cementitious beam specimen containing a single notch.

### 3 RESULTS AND DISCUSSION

Figure 2 presents a representative load vs. CMOD curve, highlighting three distinct phases: an initial elastic stage without cracking, a crack initiation and the growth of fracture process zone (FPZ) leading to peak load, and a post-peak crack propagation phase where the load drops as the crack advanced [15].

Binary images processed from DIC data provided detailed measurements of the maximum PFZ size near the crack tip for various notch locations and printing intervals. The critical effective crack length, determined by adding the initial notch size to the

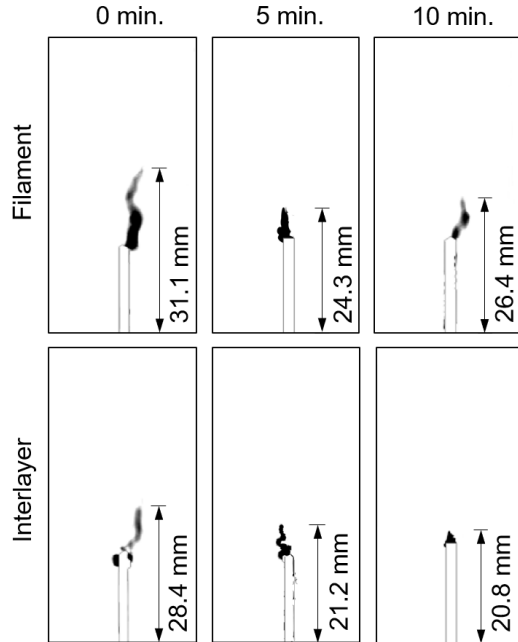
maximum FPZ size, is plotted in Figure 3. Results indicate that increasing the printing time interval significantly reduced the FPZ size and critical crack length. As the interval increased from 0 to 10 minutes, the critical crack length decreased from  $31.1 \text{ mm}$  to  $26.4 \text{ mm}$  for filament notches and from  $28.4 \text{ mm}$  to  $20.8 \text{ mm}$  for interlayer notches. These reductions were attributed to the rise in viscosity and yield stress over time during the prolonged time interval of additive manufacturing, which increased the occurrence of flaws near the crack tip, limiting FPZ growth.



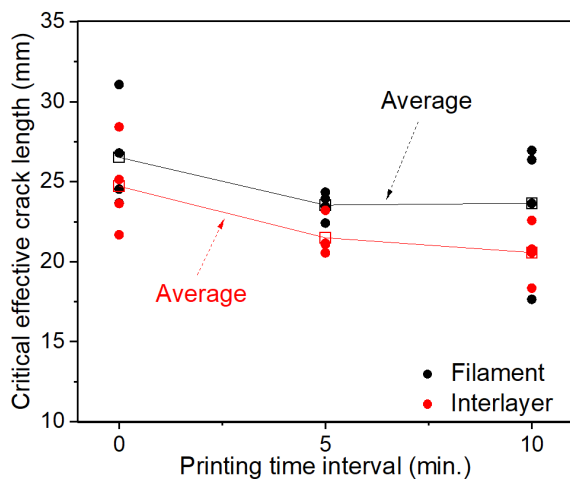
**Figure 2.** Representative fracture behavior of 3DPC: (a) load vs. CMOD relation, (b) DIC images of crack initiation and propagation at different loading stages.

Figure 4 highlights that interlayer notches exhibit a shorter critical effective crack length

compared to filament notches, implying weaker bridging by aggregates and cement grains at interlayer crack tips. This reduced bridging effect facilitates easier crack propagation through interlayers, as indicated by their smaller FPZ.



**Figure 3.** Critical effective crack length [15].



**Figure 4.** Effect of printing time interval on critical effective crack length [15].

Figure 5 shows the thixotropic behavior of additively manufactured cementitious material under varying shear rates studied through a three-stage shear test. The initial viscosity at a low shear rate of  $0.1 \text{ s}^{-1}$  decreased slightly from 1,319 to 967 Pa·s, indicating minimal

weakening of colloidal interactions. When the shear rate increased to  $15 \text{ s}^{-1}$ , the viscosity dropped sharply to 10.5 Pa·s due to the breakdown of colloidal interactions and calcium silicate hydrate (C-S-H) bonds. Upon reducing the shear rate back to  $0.1 \text{ s}^{-1}$ , the viscosity quickly recovered to 167 Pa·s and gradually increased over time, reaching 8,025 Pa·s at 15 minutes as continued C-S-H nucleation formed a rigid network. After 960 seconds, the material's viscosity increased to 8.6 times its initial value.

This thixotropic behavior led to a change in the air-phase microstructure of the additively manufactured cementitious material, especially at the interlayer region. Figure 6 shows the 3D rendering of the air phase and the calculated porosity profiles along the sample height for different printing intervals ( $t_p = 0, 5, 10,$  and  $15$  minutes). The interlayer is located at the mid-height of each sample. When  $t_p = 0$ , the porosity of the interlayer region at mid-height was similar to that of the filament region. However, as  $t_p$  increased, peak porosity in the interlayer rose significantly, reaching 30.5% at  $t_p = 15$  minutes. Additionally, the high-porosity interlayer zone expanded, indicating that longer printing intervals led to more imperfections in the interlayer, potentially compromising the fracture toughness of the interlayer region.

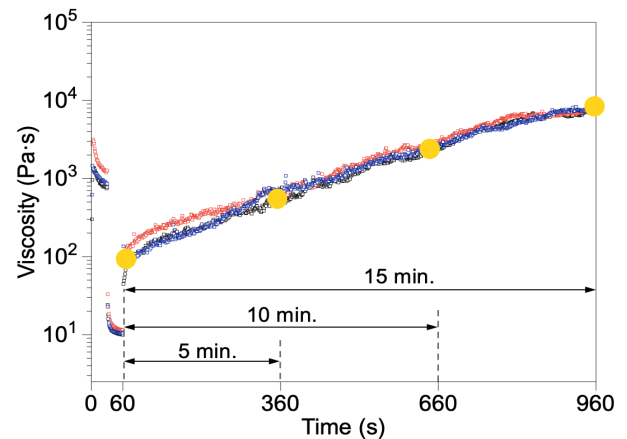


**Figure 5.** Thixotropic behavior of additively manufactured cementitious material [3].

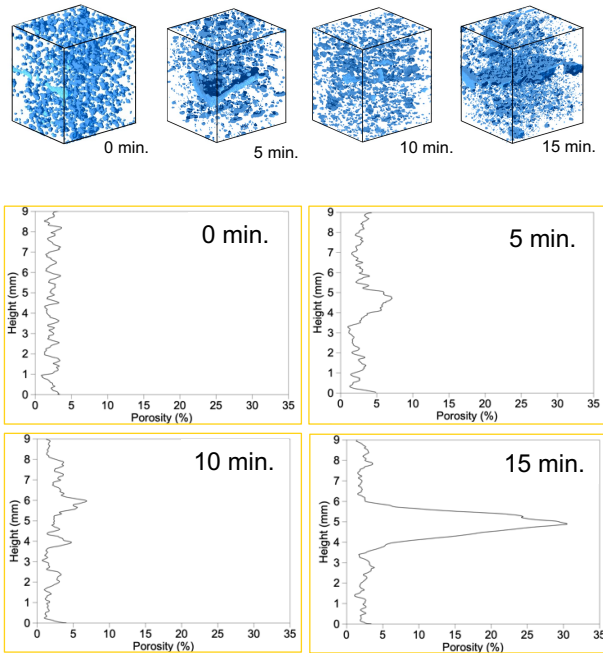


**Figure 6.** 3D rendering of air-phase structure and porosity variation along sample height for printing time intervals corresponding to 0, 5, 10 and 15 minutes on the thixotropic curve in Figure 5 [3].

The observed increase in interlayer porosity was attributed to the thixotropic behavior of the cementitious material. After extrusion and deposition, viscosity rose over time, and a longer  $t_p$  resulted in higher viscosity and greater susceptibility to defect formation in the interlayer.

Mode I fracture toughness ( $K_{IC}$ ) was determined using the peak load recorded from the load versus CMOD curve, effective crack length measured by DIC, and dimensions of each notched beam specimen. As shown in Figure 7,  $K_{IC}$  decreased by 9.4%, 17.7%, and 21.2% in average as  $t_p$  increased to 5, 10, and 15 minutes, respectively. Figures 5-7 collectively highlight the relationship among viscosity recovery, increased interlayer porosity, and reduced fracture toughness. The reduction in  $K_{IC}$  due to longer  $t_p$  is attributed to the sensitivity of interlayer porosity and defects to variations in printing intervals. This emphasizes the pivotal role of fresh-state thixotropic behavior in governing the hardened-state mechanical properties of additively manufactured cementitious materials.

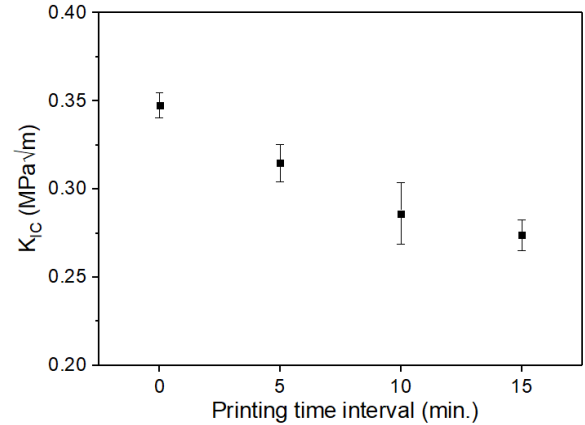


**Figure 7.** Effect of printing time interval on fracture toughness [3].

## 4 CONCLUSIONS

The following key conclusions were drawn from this study:

The introduction of interlayers in cementitious materials through the additive manufacturing process significantly affects porosity and fracture toughness  $K_{IC}$ . Interlayer regions exhibit lower  $K_{IC}$  and shorter critical crack lengths compared to filament regions, indicating that crack initiation and propagation are more likely to occur at interlayers.

The thixotropic nature of AM cementitious materials—characterized by viscosity reduction under high shear and subsequent recovery post-shear removal—plays a critical role in determining the pore structure and fracture properties of the interlayers. Longer printing intervals ( $t_p$ ) led to greater viscosity recovery, increased porosity in the interlayer region, and a consequent reduction in fracture toughness.

## REFERENCES

- [1] Roussel, N., Ovarlez, G., Garrault, S and Brumaud, C., 2012. The origins of thixotropy of fresh cement pastes. *Cement and Concrete Research*. **42**:148–157.
- [2] Jiao, D., De Schryver, R., Shi, C. and De Schutter, G., 2021. Thixotropic structural build-up of cement-based materials: A state-of-the-art review. *Cement and Concrete Composites*. **122**:104152.

- [3] Wu, Y., Wang, X. and Li, M., 2024. Role of thixotropy in interlayer microstructure and properties of additively manufactured cementitious materials. *Cement and Concrete Research*. **179**:107460.
- [4] Wolfs, R.J.M., Bos, F.P. and Salet, T.A.M, 2019. Hardened properties of 3D printed concrete: The influence of process parameters on interlayer adhesion. *Cement and Concrete Research*. **119**:132–140.
- [5] Rahul, A.V., Santhanam, M., Meena, H. and Ghani, Z., 2019. Mechanical characterization of 3D printable concrete. *Construction and Building Materials*. **227**:116710.
- [6] Le, T.T., Austin, S.A., Lim, S., Buswell, R.A., Law, R., Gibb, A.G.F. and Thorpe, T., 2012. Hardened properties of high-performance printing concrete. *Cement and Concrete Research*. **42**:558–566.
- [7] Feng, P., Meng, X., Chen, J.-F. and Ye, L., 2015. Mechanical properties of structures 3D printed with cementitious powders. *Construction and Building Materials*. **93**:486–497.
- [8] Mechtcherine, V., Nerella, V.N., Will, F., Näther, M., Otto, J. and Krause, M., 2019. Large-scale digital concrete construction – CONPrint3D concept for on-site, monolithic 3D-printing. *Automation in Construction*. **107**:102933.
- [9] Van Der Putten, J., De Volder, M., Van den Heede, P., De Schutter, G. and Van Tittelboom, K., 2020. 3D printing of concrete: the influence on chloride penetration. in: F.P. Bos, S.S. Lucas, R.J.M. Wolfs, T.A.M. Salet (Eds.), Second RILEM International Conference on Concrete and Digital Fabrication, Springer International Publishing, Cham, pp. 500–507.
- [10] Malan, J.D., van Rooyen, A.S. and van Zijl, G.P.A.G., 2022. Chloride induced corrosion and carbonation in 3D printed concrete. *Infrastructures-Basel*. **7**:1.
- [11] Tay, Y.W.D., Ting, G.H.A., Qian, Y., Panda, B., He, L. and Tan, M.J., 2019. Time gap effect on bond strength of 3D-printed concrete. *Virtual and Physical Prototyping*. **14**:104–113.
- [12] ASTM Standard E399, 2022, "Standard Test Method for Linear-Elastic Plane-Strain Fracture Toughness of Metallic Materials," ASTM International, West Conshohocken, PA, 2003.
- [13] Shah, S. P., 1990. Determination of fracture parameters ( $K_{Ic}^s$  and  $CTOD_c$ ) of plain concrete using three-point bend tests. *Materials and Structures*, **23**(6): 457-460.
- [14] Wu, Y.C., Cotrell, J. and Li, M., 2020. Interlayer effect on fracture behavior of 3D printing concrete. Second RILEM International Conference on Concrete and Digital Fabrication: Digital Concrete. pp. 537-546.
- [15] Wu, Y.C. and Li, M., 2022. Effects of Early-Age rheology and printing time interval on Late-Age fracture characteristics of 3D printed concrete. *Construction and Building Materials*. **351**: 128559.